#10

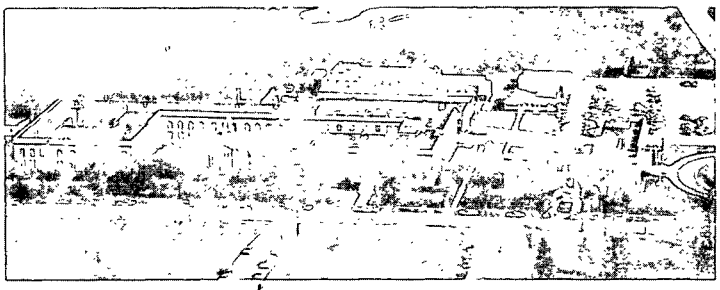

THE INSTITUTE OF PAPER CHEMISTRY, APPLETON, WISCONSIN

IPC TECHNICAL PAPER SERIES

NUMBER 10

SLOW PERMEATION OF FLUIDS THROUGH ASSEMBLAGES OF ELLIPTIC CYLINDERS

GEORGE RONALD BROWN AND HERIBERT MEYER

JUNE, 1975

SLOW PERMEATION OF FLUIDS THROUGH ASSEMBLAGES OF ELLIPTIC CYLINDERS

George Ronald Brown
Westvaco Corporation
Research Laboratory
Box 5207
North Charleston, South Carolina

Heribert Meyer
Senior Research Associate
Division of Materials Engineering & Processes
The Institute of Paper Chemistry
Appleton, Wisconsin

SLOW PERMEATION OF FLUIDS THROUGH ASSEMBLAGES OF ELLIPTIC CYLINDERS

George Ronald Brown and Heribert Meyer

INTRODUCTION

The slow permeation of fluids through porous media is a phenomenon of importance in many industrial operations. One example of a porous medium of theoretical interest is an assemblage of cylinders, which serves as a model of a fiber mat. Mats of fibers with a fluid permeating through them are found in a variety of processes, including the removal of particles from an air stream, the separation of solids from water, and the drainage of water on a paper machine forming section. Since many commonly used fibers, particularly natural ones, are not circular in cross section, the effect of the fiber cross-sectional shape on the resistance to flow through a mat is a question of interest to the analysis of flow through fiber mats.

The subject matter of flow through porous media includes a number of pertinent relationships obtained empirically or semiempirically, which can provide no insight into the effect of cross-sectional shape on the resistance to flow through arrays of cylinders. A cell model, used in the analysis of creeping flow through arrays of circular cylinders, could be applied to the slow permeation through assemblages of elliptic cylinders in order to obtain information about the influence of cross-sectional shape on the resistance to flow. An elliptic cylinder is a convenient model for analysis since the boundary is easily specified in elliptic coordinates and the shape of the cross section can be changed from circular to nearly flat simply by varying the ratio of cross-sectional axes. The extension of the cell method to the analysis of creeping flow through assemblages of elliptic cylinders is presented here.

SLOW PERMEATION OF FLUIDS THROUGH ASSEMBLAGES OF ELLIPTIC CYLINDERS

George Ronald Brown and Heribert Meyer

ABSTRACT

The slow permeation of fluids through assemblages of elliptic cylinders is analyzed by means of a zero vorticity cell model, similar to that used by Kuwabara for circular cylinders. Solutions to three directional flow boundary value problems, one along each principal cylinder axis, permit estimation of the drag on the cylinder in the cell, which leads to a measure of the resistance to flow through the assemblage. A novel approximate procedure developed herein provides an easy means of solving Poisson equations occurring in boundary value problems for which exact solutions may be intractable. The effect of the cross-sectional shape of the cylinder on flow resistance for isotropic assemblages is seen to be minimal until fairly flat cylinders are considered.

Correspondence concerning this paper should be addressed to Heribert Meyer.

SCOPE

The slow permeation of fluids through porous media is a phenomenon of importance in many industrial operations. One example of a porous medium of theoretical interest is an assemblage of cylinders, which serves as a model of a fiber mat. Mats of fibers with a fluid permeating through them are found in a variety of processes, including the removal of particles from an air stream, the separation of solids from water, and the drainage of water on a paper machine forming section. Since many commonly used fibers, particularly natural ones, are not circular in cross section, the effect of the fiber cross-sectional shape on the resistance to flow through a mat is a question of interest to the analysis of flow through fiber mats. Previous studies (Bliesner, 1964; Labrecque, 1968) indicate that such an effect might be significant, but at present the issue is unsettled.

The subject matter of flow through porous media includes a number of pertinent relationships which were obtained empirically or semiempirically, such as the Kozeny-Carman concept (Carman, 1937), which can provide no insight into the effect of cross-sectional shape on the resistance to flow through arrays of cylinders. A cell model, as used in the analyses of Happel (1959) and Kuwabara (1959) for creeping flow through arrays of circular cylinders, could be applied to the slow permeation of assemblages of elliptic cylinders in order to obtain information about the influence of cross-sectional shape of the resistance to flow. An elliptic cylinder is a convenient model for analysis since the boundary is easily specified in elliptic coordinates and the shape of the cross section can be changed from circular to nearly flat simply by varying the ratio of cross-sectional axes. The extension of the cell method to the analysis of creeping flow through assemblages of elliptic cylinders is presented herein.

CONCLUSIONS

The use of the cell model approach to study parallel or perpendicular flow past arrays of elliptic cylinders provides insight into the effect of the cross-sectional shape of the cylinders on the drag caused by such flow. While the drag due to flow past arrays of circular cylinders has been previously examined by means of the cell model method, the application of this technique to creeping flow, either parallel or perpendicular to the cylinders' central axes, past assemblages of elliptic cylinders is greatly expanded in this work. The results for flow parallel to the cylinders indicate that the influence of the cross-sectional shape on the drag is significant but not large, and the effect is porosity dependent. When the flow is perpendicular to the cylinders, two cases are considered. The drag due to flow parallel to the major cross-sectional axis is dependent to a considerable extent on the ratio of minor to major axes, or the "flatness" of the cylinders. Flow parallel to the minor axis results in drag that is more dependent on the axis ratio than for the other perpendicular flow direction. This last flow case displays a very strong dependence on the axis ratio when the cylinder becomes quite flat, e.g., an axis ratio of 1/3 or less.

The approximate procedure developed to solve the boundary value problems for both parallel and perpendicular flow cases involving Poisson equations provides a fairly easy means for obtaining an approximate solution to problems that may otherwise be intractable or laborious.

The slow permeation of a fluid through a mat of uniform synthetic fibers can be studied theoretically by combining the results from the parallel and perpendicular cell model analyses of creeping flow through arrays in a

manner dependent on the mat structure. The drag on an individual cylinder can be resolved into force components along each of the three principal axes of the cylinder. In this manner the drag past a particular fiber within the mat can be predicted from the analytical results. By determining the distribution of fiber orientations within the mat, the overall mat permeability can be estimated and the effect of changing fiber shape on permeability clarified. The Kozeny factor from the Kozeny-Carman concept of fluid flow through porous media serves as a relative indicator of the resistance to flow through a mat with other parameters constant (porosity and specific surface). For example, an isotropic mat of circular synthetic fibers of porosity 0.75 should theoretically have a Kozeny factor of 7.9, whereas if the fibers have an elliptic cross section of axis ratio 1/3 the Kozeny factor changes to 8.4; with flatter fibers the Kozeny factor increases sharply. Available experimental permeability measurements with synthetic fiber mats indicate that the actual Kozeny factors are much less than the theoretical values derived from the cell model analysis, although their trends of variation with axis ratio and porosity are similar.

The differences between the cell model analytical results and the experimental values of the Kozeny factor for synthetic fiber mats indicate that the cell method is not a good way to model flow through mats of non-circular fibers. Possibly the choice of a boundary condition other than the zero vorticity claim would make the cell model approach more suitable for fiber mats.

BACKGROUND

The fundamental relationship for slow flow through porous media is Darcy's equation, expressed by Carman (1956) as

$$\underline{U} = \underline{Q}/\underline{A} = - (\underline{K}/\mu)\, d\underline{p}/d\underline{x} \tag{1}$$

The permeability coefficient, $\underline{K}$, embodies the effect of the porous structure on the flow. The Kozeny-Carman theory (Carman, 1937), based on semiempirical reasoning, relates $\underline{K}$ to the properties of the porous medium. Introducing this concept into Darcy's equation yields

$$d\underline{p}/d\underline{x} = - \mu \underline{U} \underline{k}/\varepsilon \underline{m}^2 \tag{2}$$

where ε is the porosity, or volumetric void fraction, $\underline{m}$ is the hydraulic radius, and $\underline{k}$ is the Kozeny factor.

The slow permeation of assemblages of circular cylinders was analyzed by Happel (1959) and by Kuwabara (1959) by means of a cell model approach. A cell flow model was defined by two concentric circular cylinders, the inner one representing the surface of the solid cylinder and the outer one a virtual surface within the fluid around the solid cylinder. In setting up the boundary value problems for flow analysis, both used the no-slip condition on the solid boundary, but on the virtual surface Happel assumed zero shear stress while Kuwabara assumed zero vorticity. The question of which assumption is more physically valid remains unanswered. Happel and Brenner (1965) prefer the zero shear stress requirement, but Kirsch and Fuchs (1967a, 1967b) support the zero vorticity condition for cylinders. Both assumptions are of an artificial nature.

The analysis of creeping flow through arrays of cylinders can be applied to the slow permeation of fiber mats. The cell model concept is particularly useful to study flow through fiber mats because the geometry of the flow boundaries is so complicated and not easily described mathematically, a necessary step for rigorous hydrodynamic analysis. But the application of the Happel or Kuwabara results to fiber mats is not necessarily valid, because many fibers of practical importance, especially natural ones, are not circular in cross section. The effect of the fiber cross-sectional shape on the resistance to flow through a fiber mat is unclear, although some studies have suggested a relationship. Bliesner (1964) found some dependence of Kozeny factor, which serves as a relative indicator of flow resistance with other parameters (ε, $\underline{m}$, μ) constant, on fiber shape. Labrecque (1968) pursued the subject further, but did not resolve the issue convincingly. Another way to investigate the effect of cross-sectional fiber shape on Kozeny factor is to utilize the cell model approach and apply it to elliptic cylinders. Epstein and Masliyah (1972) have completed a cell model analysis of limited scope for the flow through arrays of elliptic cylinders. They obtained numerical solutions of the Navier-Stokes equations for perpendicular flow past an array of elliptic cylinders at low Reynolds numbers. Nearly creeping flow conditions were simulated by choosing an appropriately low Reynolds number. Their results were computed for a few combinations of axis ratio and porosity, and only perpendicular flow was considered.

An analysis of creeping flow through arrays of elliptic cylinders using a cell model technique with Kuwabara's zero vorticity condition was completed by Brown (1975) (in part as a sequel to unpublished work of the second author) and applied to the slow permeation of mats of noncircular fibers. This article summarizes the analysis briefly.

THEORETICAL ANALYSIS

The steady isothermal creeping flow of fluids through an assemblage of elliptic cylinders is analyzed in order to determine the Kozeny factor for such flow. The cell model approach considers an array of cylinders to be a collection of individual cells each composed of a solid cylinder segment surrounded by a fluid envelope. The cell which is treated analytically is an "average" of all the individual cells within the array of particles.

Two confocal ellipses serve as the typical cell, the inner one representing the surface of the solid cylinder segment and the outer one a virtual fluid surface. The position of the outer surface is such that the ratio of fluid volume to cell volume equals the assemblage's porosity. On the solid surface, the no-slip condition is assumed, while on the virtual surface the conditions of zero normal velocity and zero vorticity are assumed. The zero vorticity requirement is used rather than Happel's zero shear stress condition because of the simpler mathematics; the zero shear stress requirement would have led to an intractable problem. The cell model and the elliptic cylindrical coordinate system used in the analysis are illustrated in Fig. 1. The coordinates $(\xi, \eta, \underline{z})$ describe an orthogonal curvilinear system. The surfaces ξ = constant are ellipses of focal length $\underline{c}$, while the surfaces η = constant are confocal hyperbolas. The inner and outer cell ellipses are identified as ξ_0 and ξ_1, respectively. For a description of this and other curvilinear coordinate systems, see Happel and Brenner (1965). The cross-sectional axes $\underline{a}_0$, $\underline{b}_0$, and $\underline{a}_1$, $\underline{b}_1$, are for the ellipses ξ_0 and ξ_1, respectively, with $\underline{a} > \underline{b}$. The axis ratio β is defined as the ratio of $\underline{b}$ to $\underline{a}$: $\beta_0 = \underline{b}_0/\underline{a}_0$. The elliptic and Cartesian coordinates are related by

$$\underline{x} = \underline{c} \cosh \xi \cos \eta \qquad \underline{y} = \underline{c} \sinh \xi \sin \eta \qquad (3)$$

and the metric coefficient, $\underline{h}$, for this coordinate system is

$$1/\underline{h} = \underline{c}(\sinh^2\xi + \sin^2\eta)^{1/2} \tag{4}$$

[Fig. 1 here]

Three cases of flow relative to the cell are of interest: flow perpendicular to the cylinder's central axis and parallel to each of the cross-sectional axes, and flow parallel to the cylinder's central axis.

PARALLEL FLOW

The analysis of steady creeping flow parallel to the central axis of the elliptic cylinder ($\underline{z}$-direction) in the cell requires that only one pressure gradient, $d\underline{p}/d\underline{z}$, and one velocity component, $\underline{v}_{\underline{z}}$, be accounted for. The equation of continuity for this case is

$$\partial(\underline{v}_{\underline{z}}/\underline{h}^2)/\partial\underline{z} = 0 \tag{5}$$

The equation of motion reduces to

$$-d\underline{p}/d\underline{z} + \mu\nabla^2\underline{v}_{\underline{z}} = 0 \tag{6}$$

where

$$\nabla^2 = \underline{h}^2(\partial^2/\partial\xi^2 + \partial^2/\partial\eta^2) \tag{7}$$

Rearranging, the equation to be solved is

$$\partial^2\underline{v}_{\underline{z}}/\partial\xi^2 + \partial^2\underline{v}_{\underline{z}}/\partial\eta^2 = (d\underline{p}/d\underline{z})(\underline{c}^2/\mu)(\sinh^2\xi + \sin^2\eta) = \underline{f}(\xi,\eta) \tag{8}$$

subject to the boundary conditions

$$\underline{v}_{\underline{z}} = 0 \qquad \text{on } \xi = \xi_o \tag{9}$$

$$\partial\underline{v}_{\underline{z}}/\partial\xi = 0 \qquad \text{on } \xi = \xi_1 \tag{10}$$

The first is the no-slip requirement on the solid surface, while the second satisfies both the zero vorticity and zero shear stress conditions for the virtual surface. This equation is a Poisson equation, and exact and approximate solutions have been determined.

The exact solution is developed using a traditional Green's function method. The velocity reduces to

$$\underline{v}_{\underline{z}} = -(\underline{c}^2/\mu)(d\underline{p}/d\underline{z})\,\underline{X}_{\underline{E}} \tag{11}$$

$$\underline{X}_{\underline{E}} = \sum_{\substack{\underline{j}=1 \\ \text{odd}}}^{\infty} \sin[\gamma(\xi-\xi_o)][(-1)^{(\underline{j}-1)/2}\, 2 \sinh 2\xi_1 + \gamma \cosh 2\xi_o - \gamma \cos 2\eta]/[\delta\gamma^2(\gamma^2+4)] \tag{12}$$

with $\delta = (\xi_1 - \xi_o)$ and $\gamma = (\underline{j}\pi/2\delta)$.

The approximate solution for the Poisson equation is obtained by assuming a third degree polynomial for the velocity distribution

$$\underline{v}_{\underline{z}} = \alpha_1(\xi-\xi_o)/\delta + \alpha_2(\xi-\xi_o)^2/\delta^2 + \alpha_3(\xi-\xi_o)^3/\delta^3 \tag{13}$$

The coefficients α_1, α_2, and α_3 are functions of η determined so that the boundary conditions are satisfied. In addition to the boundary conditions, a solution would also satisfy the equations

$$\left.\begin{aligned} \partial \underline{v}_{\underline{z}}/\partial\eta &= 0 \\ \partial^2 \underline{v}_{\underline{z}}/\partial\eta^2 &= 0 \end{aligned}\right\} \quad \text{on } \xi = \xi_o \tag{14, 15}$$

and Equation (8) provides

$$\partial^2 \underline{v}_{\underline{z}}/\partial\xi^2 = \underline{f}(\xi_o,\eta) \qquad \text{on } \xi = \xi_o \tag{16}$$

Using these equations and the boundary conditions, the velocity distribution reduces to

$$\underline{v}_z = \underline{f}(\xi_o,\eta)[(\xi-\xi_o)^2/2 - (\xi-\xi_o)^3/(3\delta)] + \underline{g}_{(z)}(\eta)[(\xi-\xi_o) - (\xi-\xi_o)^3/(3\delta^2)] \tag{17}$$

Equation (8), the Poisson equation, is integrated from ξ_o to ξ_1; with the second boundary condition this process yields the following:

$$\frac{d^2}{d\eta^2}\int_{\xi_o}^{\xi_1} \underline{v}_z \, d\xi - \underline{g}_{(z)}(\eta) - \int_{\xi_o}^{\xi_1} \underline{f}(\xi,\eta)\, d\xi = 0 \tag{18}$$

where, here and in Equation (17),

$$\underline{g}_{(z)}(\eta) = (\partial \underline{v}_z/\partial\xi)_{\xi=\xi_o} \tag{19}$$

The function $\underline{g}_{(z)}(\eta)$ is found by introducing Equation (17) for $\underline{v}_z$ and seeking a particular solution that is periodic with π because of the flow symmetry. The resulting velocity distribution is

$$\underline{v}_z = -(\underline{c}^2/\mu)(d\underline{p}/dz)\,\underline{X}_A \tag{20}$$

$$\left.\begin{aligned}\underline{X}_A = (\sinh^2\xi_o + \sin^2\eta)[-(\xi-\xi_o)^2/2 + (\xi-\xi_o)^3/(3\delta)] \\ + [(\xi-\xi_o) - (\xi-\xi_o)^3/(3\delta^2)][(\sinh 2\xi_1 - \sinh 2\xi_o)/4 \\ - (\delta^3 + 3\delta)(\cos 2\eta)/(10\,\delta^2 + 6)]\end{aligned}\right\} \tag{21}$$

The flow rate through the annular region between the two cylinders is given by

$$\underline{Q} = (\underline{U}/\epsilon)\pi(\underline{a}_1\underline{b}_1 - \underline{a}_o\underline{b}_o) \tag{22}$$

as well as by

$$\underline{Q} = \int_0^{2\pi} \int_{\xi_o}^{\xi_1} \underline{v}_z \, \underline{h}^{-2} \, d\xi \, d\eta \tag{23}$$

Equating these two provides an equation for the pressure gradient, $d\underline{p}/d\underline{z}$, which with the Kozeny-Carman equation leads to the Kozeny factor, $\underline{k}$. The hydraulic radius, $\underline{m}$, is

$$\underline{m} = \pi(\underline{a}_1\underline{b}_1 - \underline{a}_o\underline{b}_o)/\underline{C} \tag{24}$$

where $\underline{C}$ is the circumference of the solid ellipse,

$$\underline{C} \cong \pi \, \underline{a}_o \, \underline{H} \tag{25}$$

with

$$\underline{H} \approx (3 + 10\,\beta_o + 3\beta_o^2)/[4(1 + \beta_o)] \tag{26}$$

The Kozeny factor for parallel flow is

$$\underline{k}_{(\underline{z})} = \beta_o^3\varepsilon^3/[(1-\varepsilon)^3 \, \underline{H}^2 \, (1-\beta_o^2)^2 \, \underline{P}^*] \tag{27}$$

where $\underline{P}^*$ is dependent on the solution used. For the exact solution $\underline{P}^*$ equals

$$\underline{P}^*_{\underline{E}} = \sum_{\substack{j=1 \\ \text{odd}}}^{\infty} \Big\{ 4[\alpha_o \, (-1)^{(j-1)/2} + (\gamma/2)(1+\beta_o^2)/(1-\beta_o^2)]^2 + (\gamma^2+4)/2 \Big\} / [\gamma^2(\gamma^2 + 4)] \tag{28}$$

while for the approximate solution $\underline{P}^*$ is

$$\underline{P}^*_{\underline{A}} = \beta_o^2[\delta/3 - 1/(4\delta) + (1-\varepsilon)(1/\underline{D} - 1/\beta_o)/(8\delta^2)]/[(1-\beta_o^2)^2(1-\varepsilon)^2]$$
$$+ \beta_o(1+\beta_o^2)[-\delta^2/12 + 1/4 - (1-\varepsilon)(1/\underline{D} - 1/\beta_o)/(8\delta)]/[(1-\beta_o^2)^2(1-\varepsilon)]$$
$$+ \delta^3/(12 + 20\,\delta^2) \tag{29}$$

where

$$\alpha_o = 2\,\beta_o/[(1-\varepsilon)(1-\beta_o^2)] \tag{30}$$

$$\underline{D} = (1-\varepsilon)(\sqrt{1 + 1/\alpha_o^2} - 1/\alpha_o) \tag{31}$$

PERPENDICULAR FLOW

The steady creeping flow past the elliptic cylinder of a cell perpendicular to the cylinder's central axis is a two-dimensional problem described by the 'biharmonic' equation

$$\nabla^2(\underline{h}^2\nabla^2\psi) = 0 \tag{32}$$

where the Laplacian operator is defined by

$$\nabla^2 = \partial^2/\partial\xi^2 + \partial^2/\partial\eta^2 \tag{33}$$

and where the stream function, ψ, is related to the fluid velocity components by:

$$\underline{v}_\xi/\underline{h} = \partial\psi/\partial\eta \qquad \underline{v}_\eta/\underline{h} = -\,\partial\psi/\partial\xi \tag{34}$$

The perpendicular flow case is divided into two separate problems for analysis, that is, flow parallel to each of the two cross-sectional axes.

Assume the solid cylinder is moving with velocity $\underline{U}$ in the direction of its minor cross-sectional axis ($\underline{y}$-direction) while the surrounding fluid is at rest. The no-slip condition on the solid surface provides that $\underline{v}_{\underline{y}} = \underline{U}$ and $\underline{v}_{\underline{x}} = 0$ on $\xi = \xi_o$. These conditions transform to

$$\left.\begin{aligned} \partial\psi/\partial\eta &= \underline{U}\,\underline{c}\,\cosh\xi\,\sin\eta \qquad (35)\\ \partial\psi/\partial\xi &= -\,\underline{U}\,\underline{c}\,\sinh\xi\,\cos\eta \qquad (36)\end{aligned}\right\} \text{ on } \xi = \xi_o$$

On the virtual surface, the normal velocity, $\underline{v}_\xi$, is zero, leading to

$$\partial\psi/\partial\eta = 0 \qquad \text{on } \xi = \xi_1 \tag{37}$$

and the vorticity, ω, which has only a $\underline{z}$-component,

$$\omega = -\underline{h}^2\nabla^2\psi \tag{38}$$

is zero, giving

$$\nabla^2\psi = 0 \qquad \text{on } \xi = \xi_1 \tag{39}$$

The solution to this boundary value problem is, following Happel and Brenner (1965), expressed as

$$\psi = \psi^{(1)} + \psi^{(2)} \tag{40}$$

where $\psi^{(1)}$ and $\psi^{(2)}$ satisfy

$$\nabla^2\psi^{(1)} = 0 \tag{41}$$

$$\underline{h}^2\nabla^2\psi^{(2)} = -\omega \tag{42}$$

and

$$\nabla^2\omega = 0 \tag{43}$$

Solving the Laplace equation for ω and using the zero vorticity condition on the fluid surface gives the equation

$$\omega = \underline{B}_{(\underline{y})} (\sinh\xi - \tanh\xi_1 \cosh\xi) \cos\eta \tag{44}$$

where $\underline{B}_{(\underline{y})}$ is a parameter to be determined later. By free choice

$$(\partial\psi^{(2)}/\partial\eta)_{\xi=\xi_o} = 0 \tag{45}$$

$$(\partial\psi^{(2)}/\partial\xi)_{\xi=\xi_o} = 0 \tag{46}$$

The conditions on ξ_o are satisfied by the following solution to Equation (41):

$$\psi^{(1)} = - \underline{U}\, \underline{c} \cosh \xi \cos \eta \tag{47}$$

The third boundary condition, Equation (37), leads to

$$(\partial\psi^{(2)}/\partial\eta)_{\xi=\xi_1} = - \underline{U}\, \underline{c} \cosh \xi_1 \sin \eta \tag{48}$$

which upon integrating gives

$$(\psi^{(2)})_{\xi=\xi_1} = \underline{U}\, \underline{c} \cosh \xi_1 \cos \eta \tag{49}$$

The Poisson equation resulting from Equation (42), i.e.,

$$\partial^2\psi^{(2)}/\partial\xi^2 + \partial^2\psi^{(2)}/\partial\eta^2 = - (\omega/\underline{h}^2) \tag{50}$$

needs to be solved for $\psi^{(2)}$. Integrating this over the range of ξ gives

$$\underline{g}_{(\underline{y})}(\eta) + \frac{d^2}{d\eta^2}\int_{\xi_o}^{\xi_1} \psi^{(2)}\, d\xi = -\int_{\xi_o}^{\xi_1} (\omega/\underline{h}^2)\, d\xi \tag{51}$$

where

$$\underline{g}_{(\underline{y})}(\eta) = (\partial\psi^{(2)}/\partial\xi)_{\xi=\xi_1} \tag{52}$$

Equation (51) can be used to determine $\underline{g}_{(\underline{y})}(\eta)$ once $\psi^{(2)}$ is known. An exact solution for $\psi^{(2)}$ satisfies

$$(\partial^2\psi^{(2)}/\partial\xi^2)_{\xi=\xi_o} + (\partial^2\psi^{(2)}/\partial\eta^2)_{\xi=\xi_o} = - (\omega/\underline{h}^2)_{\xi=\xi_o} \tag{53}$$

while the fourth boundary condition requires

$$\nabla^2\psi^{(2)} = 0 \qquad \text{on } \xi = \xi_1 \tag{54}$$

Assume a fourth degree polynomial for $\psi^{(2)}$ as follows:

$$\psi^{(2)} = \alpha_2(\xi-\xi_o)^2 + \alpha_3(\xi-\xi_o)^3 + \alpha_4(\xi-\xi_o)^4 + \alpha_5(\xi-\xi_o)^5 \tag{55}$$

where α_2, α_3, α_4, and α_5 are functions of η determined by using Equations (49), (50), (53), and (54). This form for $\psi^{(2)}$ is suggested by Equation (46). A solution to Equation (52) for $\underline{g}_{(\underline{y})}(\eta)$ can now be found. The factor $\underline{B}_{(\underline{y})}$ in the vorticity expression is determined by using the requirement that

$$[\nabla^2(\underline{h}^2\nabla^2\psi)]_{\xi=\xi_o} = 0 \tag{56}$$

The result is

$$\underline{B}_{(\underline{y})} = \underline{G}_{(\underline{y})}\underline{U}/\underline{c} \tag{57}$$

where $\underline{G}_{(\underline{y})}$ is as follows:

$$\underline{G}_{(\underline{y})} = \underline{R} \cosh \xi_1/\underline{T}_{(\underline{y})} \tag{58}$$

with

$$\underline{R} = [\cosh 2\xi_o\ (512 - 60/\delta^2 + 900/\delta^4) + \sinh 2\xi_o\ (\delta - 30/\delta + 600/\delta^3)]/(\delta^2 + 10) \tag{59}$$

and

$$\underline{T}_{(\underline{y})} = \sigma[\Lambda - (1/4)\Omega(\cosh 2\xi_o + 13)/(\delta^2 + 10) + (9/4)(\Omega - 7/2)/(9\delta^2 + 10) + 27\delta^2\Omega/[(\delta^2 + 10)(9\delta^2 + 10)] - 60\underline{t}_{(\underline{y})}\Omega/[\delta^3(\delta^2 + 10)] + 30\lambda[(\Omega - 7/2)/\delta^2 + 12\Omega/(\delta^2 + 10)]/[\delta(9\delta^2 + 10)] \tag{60}$$

and where

$$\sigma = (\sinh \xi_o - \tanh \xi_1 \cosh \xi_o) \tag{61}$$

$$\underline{t}_{(\underline{y})} = [\cosh^3\xi_1 - \cosh^3\xi_o - \tanh \xi_1\ (\sinh^3\xi_1 - \sinh^3\xi_o)]/3 - \tanh \xi_1\ (\sinh \xi_1 - \sinh \xi_o) \tag{62}$$

$$\lambda = [\cosh \xi_1 - \cosh \xi_o - \tanh \xi_1\ (\sinh \xi_1 - \sinh \xi_o)] \tag{63}$$

$$\Omega = (7 \cosh 2\xi_o + 4\delta \sinh 2\xi_o) \tag{64}$$

$$\Lambda = [-(1/8 + 9/4\delta^2) \cosh 4\xi_o - (9/4\delta) \sinh 4\xi_o + (3/2) \cosh 2\xi_o + 3/4 - 9/2\delta^2] \tag{65}$$

The drag force on a stationary cylinder due to flow past it is determined by integrating the stress over the solid surface, as follows (Happel and Brenner, 1965):

$$\vec{\underline{F}} = \int_{\underline{s}} \underline{\underline{\Pi}} \cdot d\vec{\underline{s}} = \int_{\underline{s}} \underline{\underline{\Pi}} \cdot \hat{i}_\xi \, d\underline{s} \tag{66}$$

where $\hat{i}_\xi$ is a unit vector normal to the solid surface and $\underline{\underline{\Pi}}$ is the stress tensor. Only the $\underline{y}$-component of $\vec{\underline{F}}$ is nonzero. After determining the stress tensor for a stationary cylinder and performing the indicated operations, the simple result is

$$\underline{F}_{(\underline{y})} = -\pi \mu \underline{U} \underline{G}_{(\underline{y})} \tag{67}$$

The drag force on the cylinder is related to the pressure drop within the cell by

$$\underline{F}/(\pi \underline{a}_1 \underline{b}_1) = d\underline{p}/d\underline{y} \tag{68}$$

where $\underline{y}$ is the direction of motion. Combining this and the Kozeny-Carman equation provides for the Kozeny factor

$$\underline{k} = -\underline{F}\varepsilon\underline{m}^2/(\pi \underline{a}_1 \underline{b}_1 \mu \underline{U}) \tag{69}$$

For perpendicular flow along the minor cross-sectional axis, the Kozeny factor is

$$\underline{k}_{(\underline{y})} = \varepsilon^3 \beta_o \underline{G}_{(\underline{y})}/[\underline{H}^2(1-\varepsilon)] \tag{70}$$

The problem for flow along the major axis of the cross section and perpendicular to the cylinder is approached as above, but the cylinder now is moving in the $\underline{x}$-direction in the still fluid. Developing the solution as above, the resulting drag force is

$$\underline{F}_{(\underline{x})} = - \pi \mu \underline{U} \underline{G}_{(\underline{x})} \tanh \xi_1 \tag{71}$$

and the Kozeny factor is

$$\underline{k}_{(\underline{x})} = \varepsilon^3 \beta_o \underline{G}_{(\underline{x})} \tanh \xi_1 / [\underline{H}^2 (1-\varepsilon)] \tag{72}$$

where

$$\underline{G}_{(\underline{x})} = - \underline{R} \sinh \xi_1 / \underline{T}_{(\underline{x})} \tag{73}$$

$$\begin{aligned} \underline{T}_{(\underline{x})} = \sigma\{ & - \Lambda + 2 \cosh 2\xi_o - 3/4 + (1/4)\Omega(\cosh 2\xi_o - 13)/(\delta^2 + 10) \\ & + 27 \delta^2 \Omega / [(\delta^2 + 10)(9\delta^2 + 10)] + (9/4)(\Omega + 7/2)/(9\delta^2 + 10)\} \\ & - 60 \underline{t}_{(\underline{x})} \Omega / [\delta^3 (\delta^2 + 10)] \\ & + 30 \lambda [(\Omega + 7/2)/\delta^2 + 12 \Omega/(\delta^2 + 10)]/[\delta(9\delta^2 + 10)] \end{aligned} \tag{74}$$

$$\begin{aligned} \underline{t}_{(\underline{x})} = & [\cosh^3 \xi_1 - \cosh^3 \xi_o - \tanh \xi_1 (\sinh^3 \xi_1 - \sinh^3 \xi_o)]/3 \\ & - (\cosh \xi_1 - \cosh \xi_o) \end{aligned} \tag{75}$$

RESULTS AND DISCUSSION

The approximate procedure used for solving the Poisson equations produces realistic results, suggesting that this technique may have applicability to other problems where a complicated Poisson equation is encountered. The accuracy of the method is tested by comparing the exact and approximate solutions for the parallel flow problem. In Fig. 2, the velocity profiles in the annulus along the $\underline{x}$ and $\underline{y}$ axes from both solutions are compared. Along the $\underline{x}$-axis, or $\eta = 0$, the two are almost identical. Along the $\underline{y}$-axis, or $\eta = \pi/2$, the two profiles are very close near the solid surface but diverge somewhat as the virtual boundary is approached. This comparison is for a cylinder of cross-sectional axis ratio of 0.50 and for a porosity of 0.75. At higher porosities the error due to the approximate solution increases, but does not become of serious concern until porosities above 0.95 are reached.

[Fig. 2 here]

No such comparison is possible to test the perpendicular flow approximate solutions, but the flow patterns can be observed for realism. Streamlines for perpendicular flow along each cross-sectional axis for a cylinder of axis ratio of 0.50 at a porosity of 0.75 are shown in Fig. 3 and 4. These patterns of flow past the cylinder are as expected.

[Fig. 3 and 4 here]

Results in terms of the directional Kozeny factors are presented in Fig. 5 for parallel flow and in Fig. 6 for perpendicular flow. The truly circular cylinder cannot be treated by the theory, so an axis ratio of 0.999 is used instead. The parallel flow results for the circular case agree well with values from the analysis of Happel (1959); this is expected since both the zero

vorticity and zero shear stress conditions are mathematically identical for parallel flow in the cell. For elliptic cylinders the parallel flow results are not strongly affected by the cross-sectional axis ratio. The perpendicular Kozeny factors for round cylinders correspond closely to those of Kuwabara (1959), which should be so since both were developed using the zero vorticity model. This agreement provides additional support for the approximate solution procedure used for this analysis. As the cylinders are flattened, two sets of Kozeny factors result, one for flow along each axis. The values for perpendicular flow along the minor axis show a strong dependence on axis ratio and porosity. Those for flow along the major axis show a lesser, but still significant, dependence on axis ratio and porosity.

[Fig. 5 and 6 here]

The Kozeny factors obtained in this analysis differ somewhat from those computed by Masliyah (1970). Figure 7 compares some values for perpendicular flow along the minor cross-sectional axis. While the nearly circular values are close, the difference becomes large for flat cylinders, e.g., an axis ratio of 0.20 or less. Since the Masliyah results are only extrapolated into the creeping flow region, the differences can be attributed to the effect of inertial forces.

[Fig. 7 here]

Applying the cell model analysis to a nonordered assemblage of cylinders, such as a fiber mat, requires a knowledge of the structure of the assemblage. The drag on a particular cylinder within such an assemblage can be resolved into force components in the direction of each of the three principal axes of the cylinder, each of which corresponds to one of the three cell model flow problems. If the orientation of the cylinder relative to the flow direction

is known, the drag on the cylinder can be estimated from the cell analysis. In this manner the resistance to flow through an array of specified geometry can be predicted. The orientation of a cylinder within an array is identified by two angles, as follows: θ is the angle between a cylinder's central axis and the normal to the plane of the mat; ϕ is the angle of rotation about the cylinder's central axis with the zero angle being when the major cross-sectional axis is parallel to the plane of the mat. Proceeding as discussed above, a composite Kozeny factor for an array is determined to be

$$\underline{k} = (\underline{k}_{(\underline{x})}\sin^2\phi + \underline{k}_{(\underline{y})}\cos^2\phi)\ \sin^2\theta + \underline{k}_{(\underline{z})}\cos^2\theta \qquad (76)$$

Several special orientations are of interest.

CASE I: All central axes parallel to flow, $\theta = 0$. The Kozeny factor is simply $\underline{k}_{(\underline{z})}$. This case is not of practical importance for fiber mats but may be for some other flow processes.

CASE II: All central axes perpendicular to flow, $\theta = \pi/2$. This case is occasionally of practical interest. Fibrous filters are often prepared so that as many fibers as possible lie in the plane of the filter (see also Case IV). Three possibilities are considered, as follows:

A: Major cross-sectional axis parallel to flow, $\phi = 0$, $\underline{k} = \underline{k}_{(\underline{x})}$.

B: Minor cross-sectional axis parallel to flow, $\phi = \pi/2$, $\underline{k} = \underline{k}_{(\underline{y})}$.

C: Cross-sectional axes at an angle to flow, $\underline{k} = \underline{k}_{(\underline{x})}\sin^2\phi + \underline{k}_{(\underline{y})}\cos^2\phi$.

CASE III: Distribution of orientations. In a real fiber mat, there is no regular ordered structure; instead the fibers assume various orientations. By identifying the orientation distribution the composite Kozeny factor can be determined in the following manner:

$$\underline{k} = \int_0^{\pi/2} (\underline{k}_{(\underline{t})}\sin^2\theta + \underline{k}_{(\underline{z})}\cos^2\theta)\ \underline{g}(\theta)\ d\theta \qquad (77)$$

where $\underline{k}_{(\underline{t})}$ is the transverse flow Kozeny factor found in a similar way:

$$\underline{k}_{(\underline{t})} = \int_0^{\pi/2} (\underline{k}_{(\underline{x})}\sin^2\phi + \underline{k}_{(\underline{y})}\cos^2\phi)\ \underline{h}(\phi)\ d\phi \qquad (78)$$

The functions $\underline{g}(\theta)$ and $\underline{h}(\phi)$ are frequency functions describing the distribution of orientation angles within the mat.

One particular distribution, that for an isotropic mat, is of interest. The choice of $\underline{g}(\theta) = \sin\theta$ provides such a mat in which the probability of a fiber end falling at any point on a sphere around the fiber center is constant. By choosing $\underline{h}(\phi) = 2/\pi$, all values of ϕ between 0 and $\pi/2$ are equally probable. This choice produces an isotropic mat in which there is no preferred cross-sectional arrangement. The composite Kozeny factor for this mat is

$$\underline{k} = (1/3)(\underline{k}_{(\underline{x})} + \underline{k}_{(\underline{y})} + \underline{k}_{(\underline{z})}) \qquad (79)$$

Using this equation to compute the Kozeny factor, the dependence of $\underline{k}$ for an isotropic mat on the fiber cross-sectional shape is seen in Fig. 8 for several porosities. Notice the relative insensitivity of $\underline{k}$ until a fairly flat cylinder (a small axis ratio) is considered. For example, at a porosity of 0.90, a mat of fibers of axis ratio 0.10 has a Kozeny factor only slightly different from that for a mat of circular fibers. At 0.75 porosity, the fibers can be flattened to near 0.30 axis ratio before a ten percent change in $\underline{k}$ occurs. Lord (1955) experimentally determined the Kozeny factors for air permeation through carefully randomized mats which should approximate the isotropic case. Figure 9 shows data for nearly circular silk fibers compared to the composite Kozeny factor curve for an isotropic mat of circular fibers. The experimental

and theoretical curves are similar, but the former is considerably lower, indicating that there is actually less resistance to flow than the cell model theory predicts.

[Fig. 8 and 9 here]

CASE IV: A mat formed slowly from a dilute fiber suspension has the fibers generally in the mat plane. For such a mat, average θ and ϕ values can be chosen to use in Equation (76) for the composite $\underline{k}$ value. The choices $\theta = 75°$ and $\phi = 20°$ seem reasonable, yielding

$$\underline{k} = 0.067\ \underline{k}_{(z)} + 0.109\ \underline{k}_{(x)} + 0.824\ \underline{k}_{(y)} \qquad (80)$$

The θ value is an estimate from the work of Elias (1965); the choice of ϕ is a guess. This mat is of interest because it approximates the mats formed by Bliesner in his permeation experiments with noncircular fibers, as well as the mats used for the Davies-Ingmanson empirical correlation with circular fibers (Ingmanson, et al., 1959). The Kozeny factors computed from Equation (80) are expected to be valid for these mats.

Consider flow through mats of circular fibers. Figure 10 presents Bliesner's experimental data, the isotropic and oriented $\underline{k}$ curves, and the Davies-Ingmanson correlation. As with the Lord data, the expected mat Kozeny factors determined from the cell model theory using Equation (80) are greater than the experimental values, although the trend with porosity is the same. The data agree fairly well with previous measurements, as represented by the correlation. Two reasons may account for this discrepancy, one an experimental problem and one a theoretical defect. Experimentally, a truly uniform mat cannot be obtained; instead any real mat contains local regions of resistance lower than the rest of the mat because of pinholes, fiber curling, uneven

deposition of fibers, edge effects, etc. Since the fluid follows paths of least action, these areas of imperfections have a stronger influence on flow properties than the average volume fraction might indicate. As a result of this, the experimentally measured Kozeny factors fall below the theoretically predicted ones obtained assuming uniform mats. The second reason for the discrepancy concerns the cell model approach where flow past a fiber segment is studied. Areas of fiber contacts are not considered, although two fibers crossing or in close proximity to each other cause less drag than if the two segments were apart. Thus the theoretical analysis over-predicts the resistance in a fiber mat, with the error increasing as the porosity decreases since then fiber contacts increase. This error due to fiber crossings also should be larger for flatter fibers, indicating that the difference between theory and experiment is dependent on the fiber axis ratio.

[Fig. 10 here]

The data of Bliesner for noncircular fibers are compared to the (cell model) theoretical estimates in Fig. 11. As for the circular fibers, the empirical Kozeny factors are considerably smaller than the expected values found from Equation (80). The difference between the two seems to increase as the fibers become flatter, which is expected on the basis of the fiber crossing argument above.

[Fig. 11 here]

The effect of axis ratio on Kozeny factor is more obvious in Fig. 12. While this graph represents a porosity of 0.75, other porosities show similar results. The composite Kozeny factor for an isotropic fiber mat is not greatly affected by the cross-sectional axis ratio until a fairly flat fiber is used. The experimental data follow the same pattern; for the range covered

by the tests the fiber axis ratio seems to have little effect on k. The assumption that the Kozeny factor of a real mat is independent of fiber cross-sectional shape, at least for axis ratios more circular than 0.2 and for higher porosities, should be valid for the permeation analysis.

[Fig. 12 here]

The significant differences between the theoretical Kozeny factors and the experimentally determined values indicate that the zero vorticity cell approach to the permeation of arrays of elliptic cylinders is not a reliable representation of the actual situation. But because of the geometric complexity of such arrays, a better flow model has not yet been worked out. Perhaps the cell analysis can be improved to account for flow in the regions of fiber contacts. Or perhaps the zero voriticity assumption is not valid for this case, and another condition could be chosen that is physically sound and would produce better agreement between theory and experiment. Obviously further work in this area would be beneficial.

The above experimental Kozeny factors were computed assuming that all the surface area of the fibers was wetted by the permeating fluid. Both Bliesner and Labrecque realized that some area is excluded from the fluid because of interfiber contacts, and they devised methods for correcting their surface area values used in the Kozeny factor calculations. The approach used by these two investigators ignored the dependence of interfiber contact area on the stress applied to the mat. A new analysis (Brown) considering this aspect indicates that, for their fiber mats, the area correction is insignificant. Therefore, the experimental k's presented above have not been corrected for interfiber contact area.

LITERATURE CITED

Bliesner, W. C., A study of the porous structures of fibrous sheets using permeability techniques, Tappi 47, no. 7: 392-400 (1964).

Brown, G. R. Creeping flow of fluids through assemblages of elliptic cylinders and its application to the permeability of fiber mats. Doctor's Dissertation, Appleton, Wisconsin, The Institute of Paper Chemistry, 1975.

Carman, P. C., Fluid flow through granular beds, Trans. Inst. Chem. Engrs. (London) 15: 150-66 (1937).

Carman, P. C. Flow of gases through porous media. New York, Academic Press, Inc., 1956.

Elias, T. C. An investigation of the compression response of ideal unbonded fibrous structures by direct observation. Doctor's Dissertation, Appleton, Wisconsin, The Institute of Paper Chemistry, 1965.

Epstein, N., and Masliyah, J. H., Creeping flow through clusters of spheroids and elliptical cylinders, Chem. Eng. J. (London) 3, no. 2: 169-75 (1972).

Happel, J., Viscous flow relative to arrays of cylinders, AIChE Journal 5, no. 2: 174-7 (1959).

Happel, J., and Brenner, H. Low Reynolds number hydrodynamics. Englewood Cliffs, N. J., Prentice-Hall, 1965.

Ingmanson, W. L., Andrews, B. D., and Johnson, R. C., Internal pressure distributions in compressible mats under fluid stress, Tappi 42, no. 10: 840-9 (1959).

Kirsch, A. A., and Fuchs, N. A., The fluid flow in a system of parallel cylinders perpendicular to the flow direction at small Reynolds numbers, J. Phys. Soc. Japan 22, no. 5: 1251-5 (1967a).

Kirsch, A. A., and Fuchs, N. A., Studies on fibrous aerosol filters — II. Pressure drops in systems of parallel cylinders, Ann. Occup. Hyg. 10: 23-30 (1967b).

Kuwabara, S., The forces experienced by randomly distributed parallel circular cylinders or spheres in a viscous flow at small Reynolds numbers, J. Phys. Soc. Japan 14, no. 4: 527-32 (1959).

Labrecque, R. P., The effects of fiber cross-sectional shape on the resistance to the flow of fluids through fiber mats, Tappi 51, no. 1: 8-15 (1968).

Lord, E., Air flow through plugs of textile fibers. Part I. General flow relations, J. Text. Inst. 46: T191-213 (1955).

Masliyah, J. H. Symmetric flow past orthotropic bodies: single and clusters. Doctor's Dissertation, Vancouver, B.C., University of British Columbia, 1970.

NOMENCLATURE

A = cross-sectional area of porous bed presented to flow

$B_{(y)}$ = factor in vorticity equation for perpendicular flow (y-direction)

C = circumference of ellipse

D = factor defined by Equation (31)

F = drag force on cylinder

$F_{(x)}$ = drag force due to x-direction flow

$F_{(y)}$ = drag force due to y-direction flow

$G_{(x)}$ = factor defined by Equation (73)

$G_{(y)}$ = factor defined by Equation (58)

H = circumference factor

K = permeability coefficient

P^*, P^*_A, P^*_E = defined quantities in parallel flow analysis

Q = volumetric flow rate

R = factor defined by Equation (59)

$T_{(x)}$ = factor defined by Equation (74)

$T_{(y)}$ = factor defined by Equation (60)

U = superficial velocity = Q/A

X_A, X_E = factors in parallel flow velocity solutions

a_o, b_o = half-axes of inner ellipse in cell model

a_1, b_1 = half-axes of outer ellipse in cell model

c = focal length of ellipse

d/dx = ordinary derivative

f = function of ξ and η

$g(\theta)$ = frequency function

$g_{(y)}$ = function of η in perpendicular flow (y-direction) solution

$g_{(z)}$ = function of η in parallel flow approximate solution

$\underline{h}$ = metric coefficient

$\underline{h}(\phi)$ = frequency function

$\underline{i}$ = unit vector normal to elliptic surface

$\underline{j}$ = integer index

$\underline{k}$ = Kozeny factor

$\underline{k}_{(\underline{t})}$ = transverse flow Kozeny factor

$\underline{k}_{(\underline{x})}, \underline{k}_{(\underline{y})}, \underline{k}_{(\underline{z})}$ = directional flow Kozeny factors

$\underline{m}$ = hydraulic radius

$\underline{p}$ = pressure

$\underline{s}$ = distance along a curve

$\underline{t}_{(\underline{x})}$ = factor defined by Equation (75)

$\underline{t}_{(\underline{y})}$ = factor defined by Equation (62)

$\underline{v}_{\underline{\xi}}, \underline{v}_{\underline{\eta}}$ = velocity components

$\underline{v}_{\underline{x}}, \underline{v}_{\underline{y}}, \underline{v}_{\underline{z}}$ = velocity components

$\underline{x}, \underline{y}, \underline{z}$ = Cartesian coordinates

α_o = factor defined by Equation (30)

$\alpha_1, \alpha_2, \alpha_3$ = factors dependent on η in parallel flow polynomial for velocity

$\alpha_2, \alpha_3, \alpha_4, \alpha_5$ = factors dependent on η in perpendicular flow ($\underline{y}$-direction) polynomial for $\psi^{(2)}$

∇^2 = Laplacian operator

β_o = $\underline{b}_o/\underline{a}_o$ = axis ratio of elliptic cross section

δ = $(\xi_1 - \xi_o)$

$\partial/\partial\underline{x}$ = partial derivative

ε = porosity or volumetric void fraction

γ = $(\underline{j}\pi/2\delta)$

λ = factor defined by Equation (63)

Λ = factor defined by Equation (65)

μ = dynamic viscosity of fluid

ω = vorticity

Ω = factor defined by Equation (64)

$\underline{\underline{\Pi}}$ = stress tensor

ϕ = angle of rotation about α, cylinder's central axis

ψ = stream function

$\psi^{(1)}$ = part of stream function in perpendicular flow that satisfies Laplace equation

$\psi^{(2)}$ = part of stream function in perpendicular flow from particular solution to Poisson equation

σ = $(\sinh \xi_o - \tanh \xi_1 \cosh \xi_o)$

θ = angle between a cylinder's central axis and the normal to the plane of the mat

ξ, η = confocal elliptic coordinates

ξ_o, ξ_1 = elliptic surfaces representing solid cylinder and virtual fluid boundary, respectively

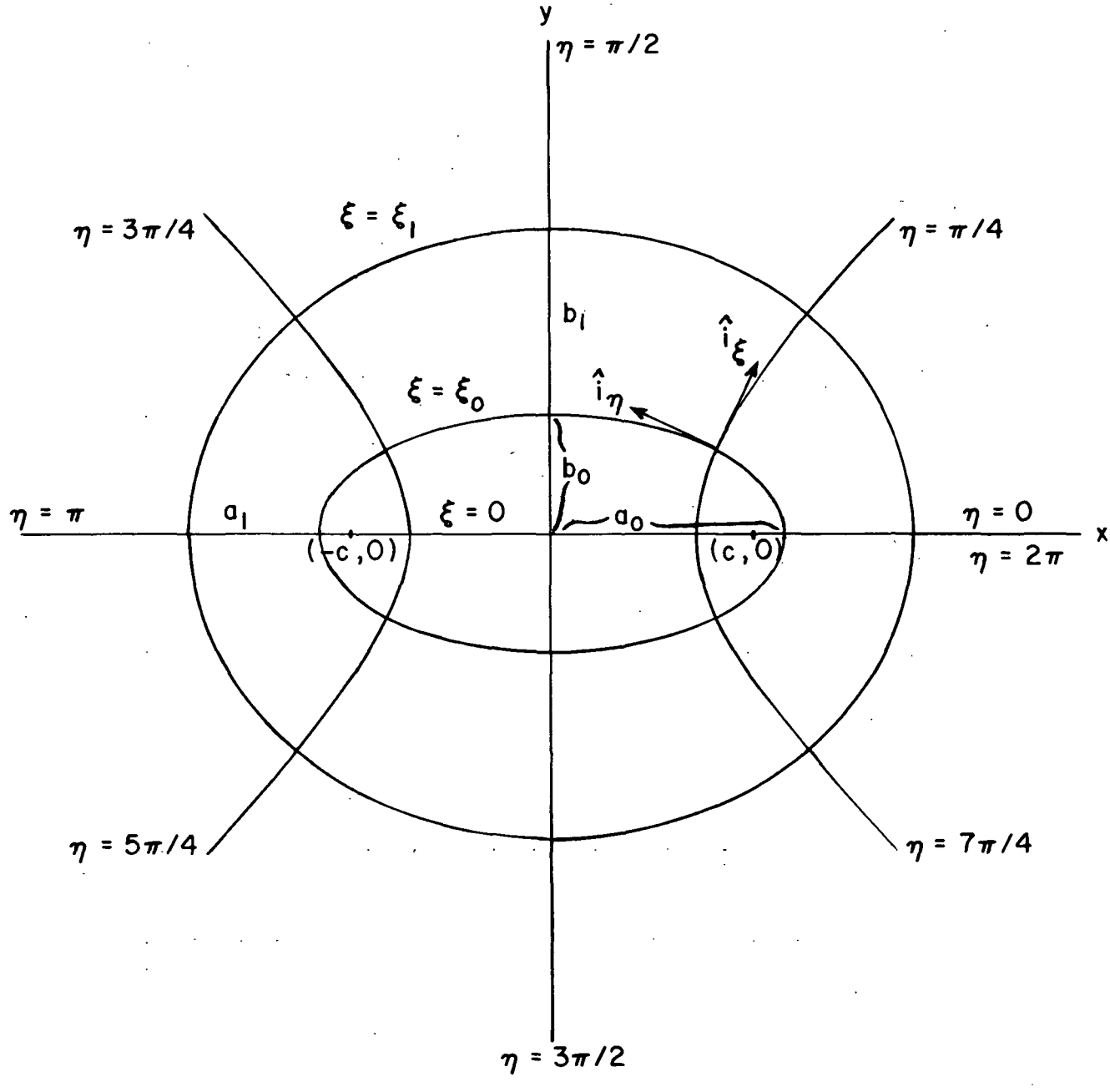

Fig. 1. Cell Flow Model Showing Two Confocal Elliptic Cylinders in Cross Section and Elliptic Coordinates.

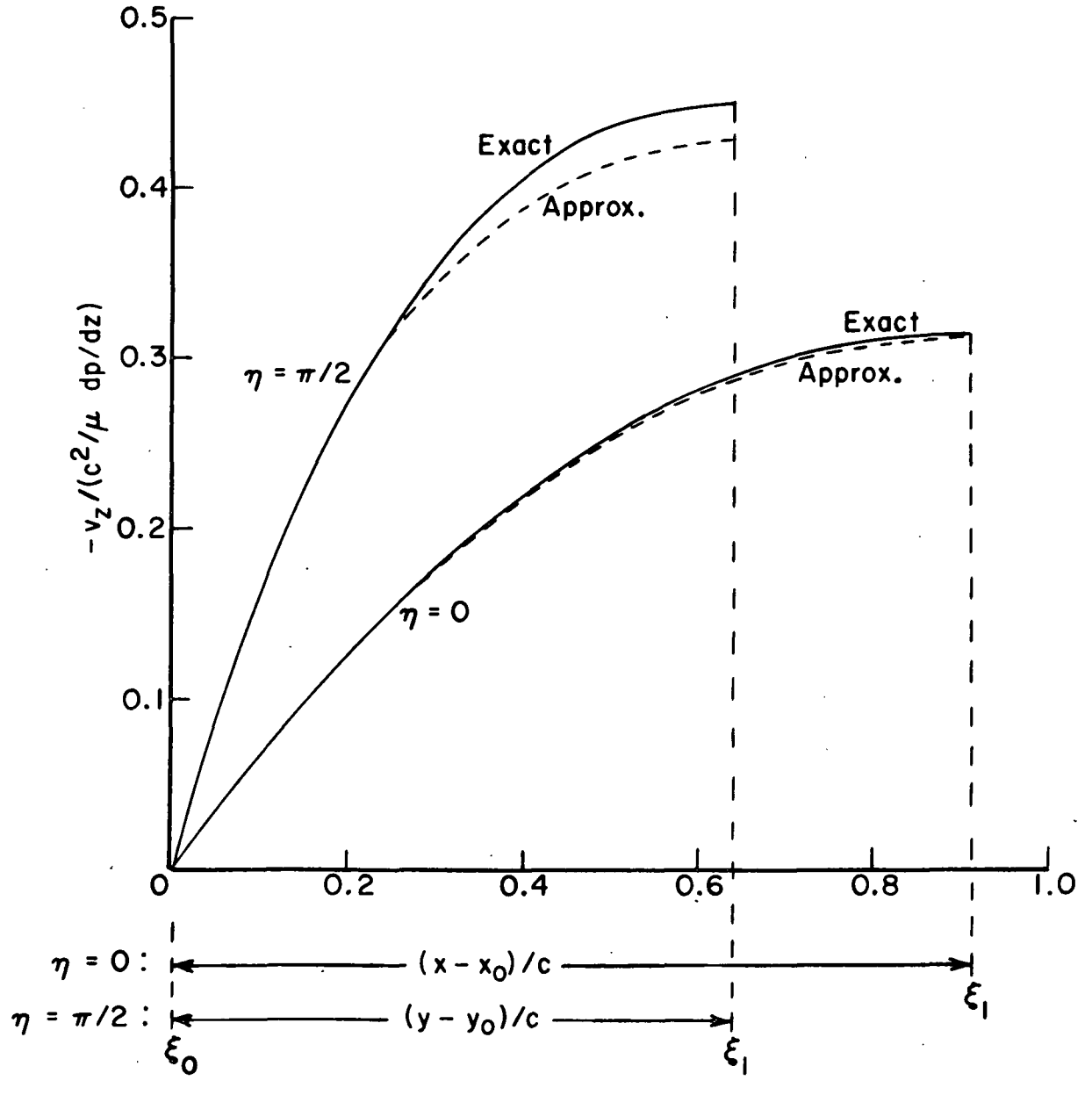

Fig. 2. Velocity Distribution in Annulus of Cell Model for Flow Parallel to Elliptic Cylinder.

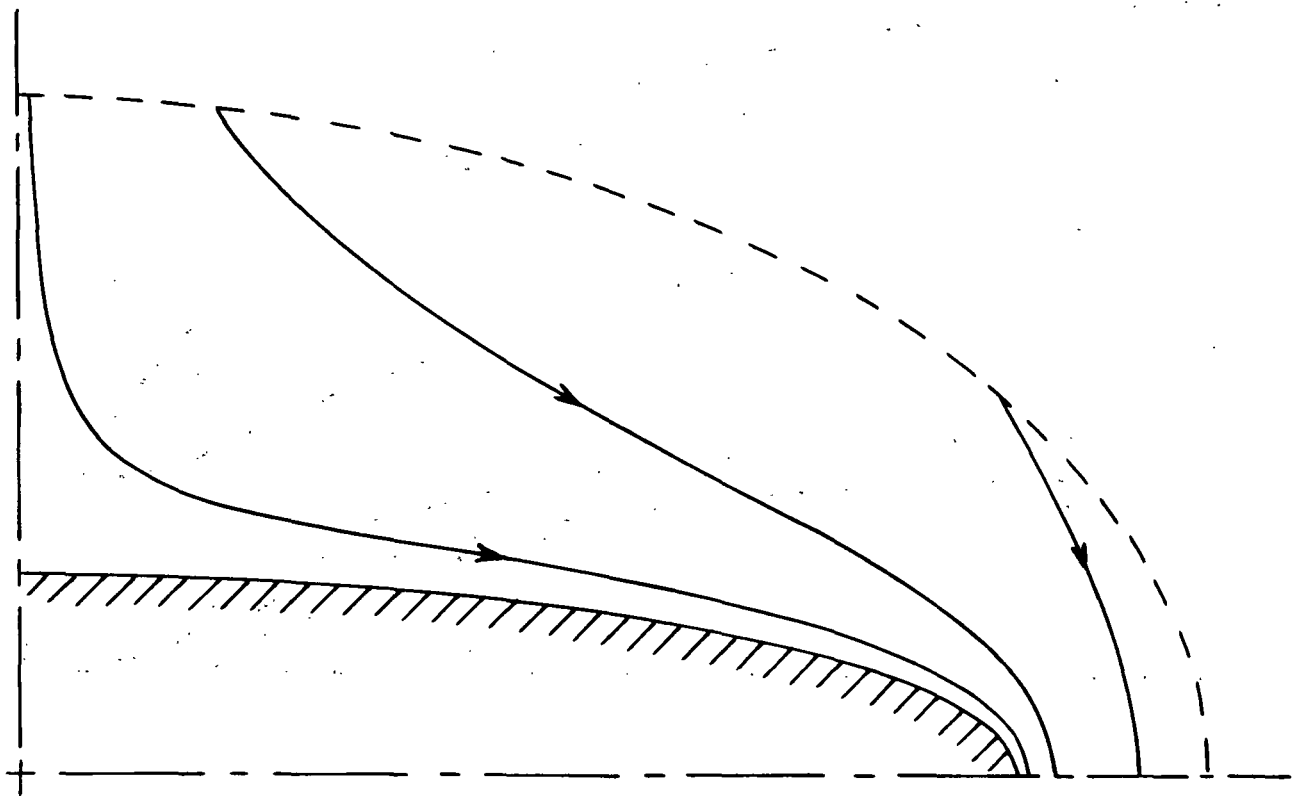

Fig. 3. Streamlines in Model Cell for Perpendicular Flow Along Minor Cross-Sectional Axis. Porosity = 0.75, Axis Ratio = 0.200.

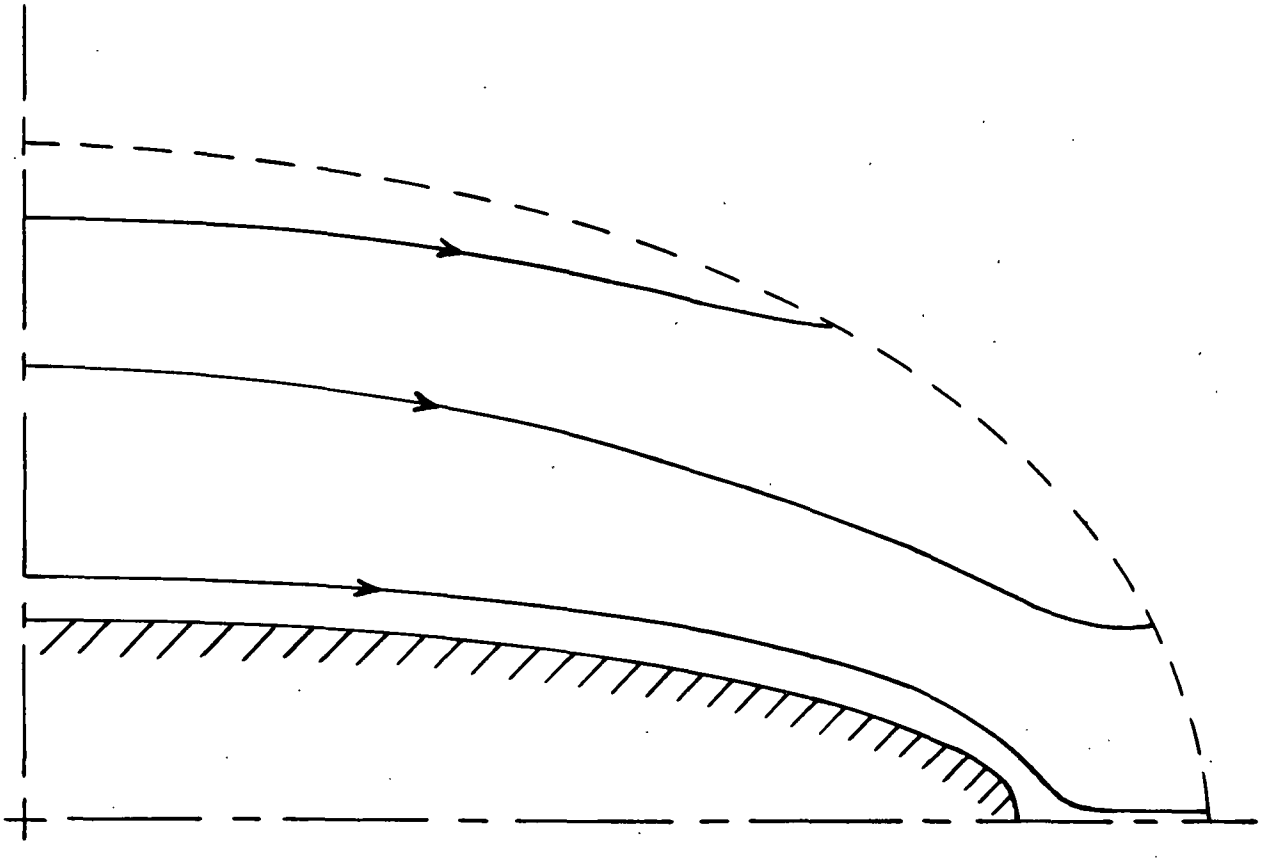

Fig. 4. Streamlines in Model Cell for Perpendicular Flow Along Major Cross-Sectional Axis. Porosity = 0.75, Axis Ratio = 0.200.

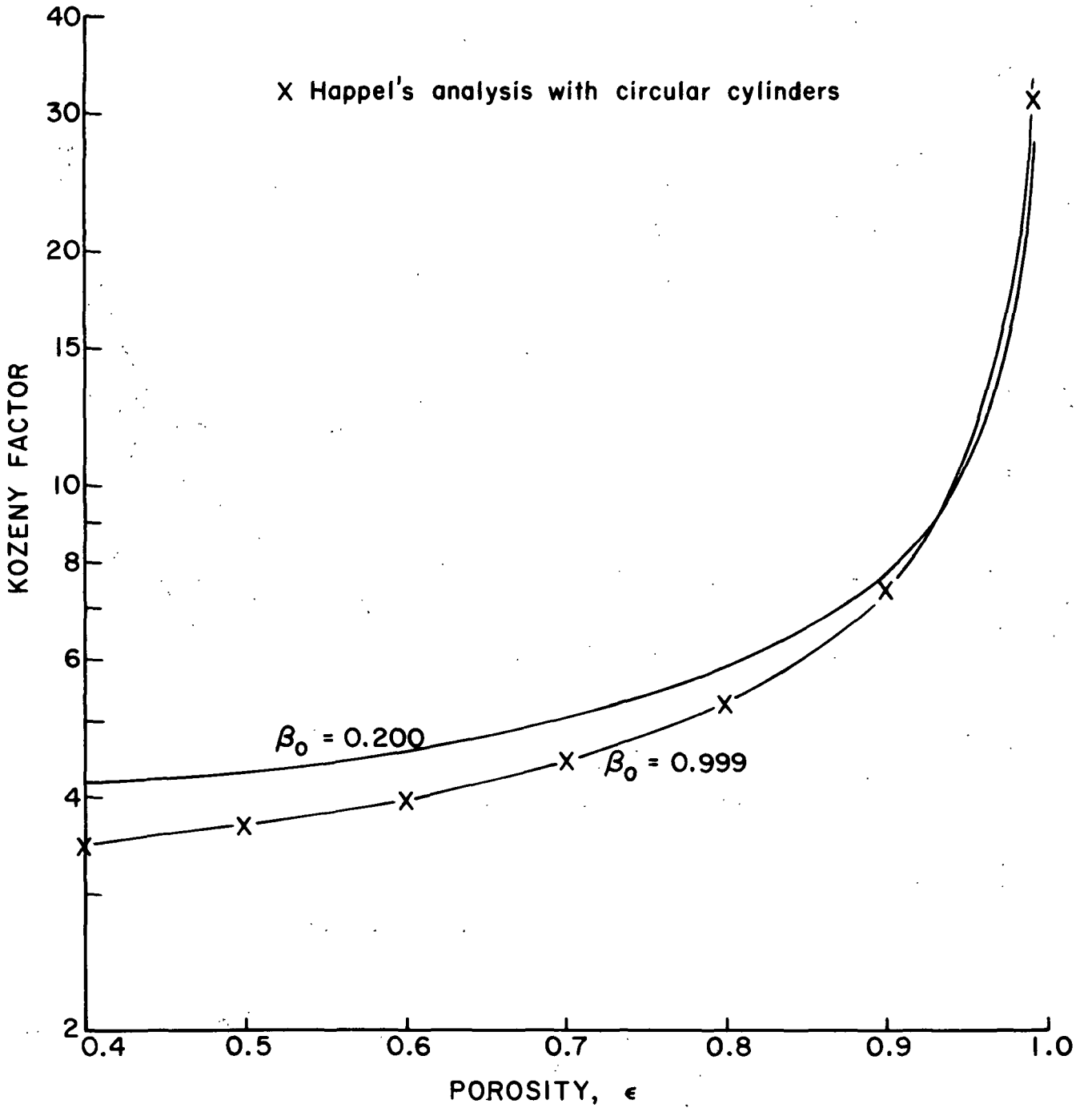

Fig. 5. Theoretical Kozeny Factors for Parallel Flow as a Function of Porosity.

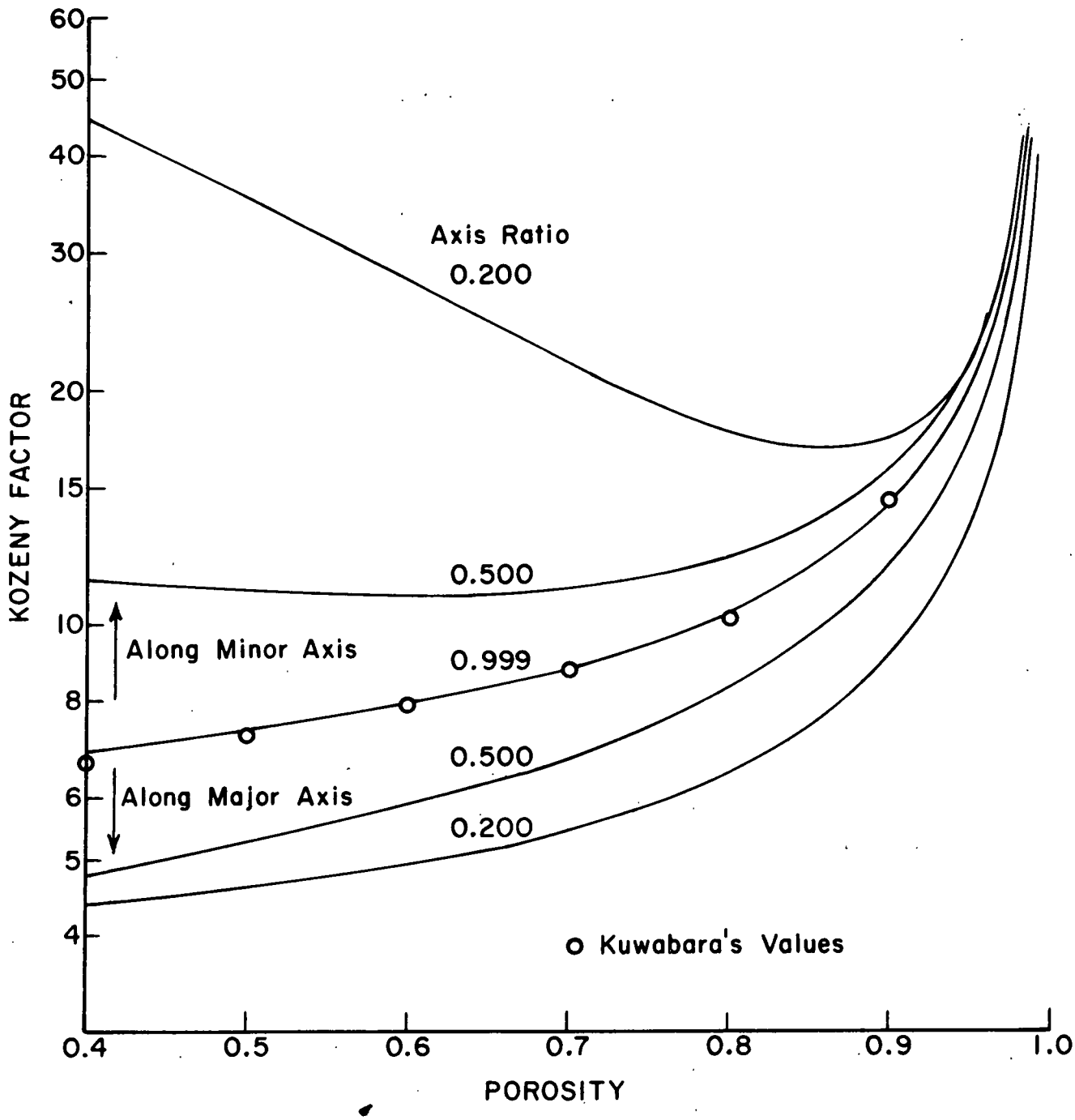

Fig. 6. Perpendicular Flow Kozeny Factors from Creeping Flow Zero Vorticity Cell Model Analysis.

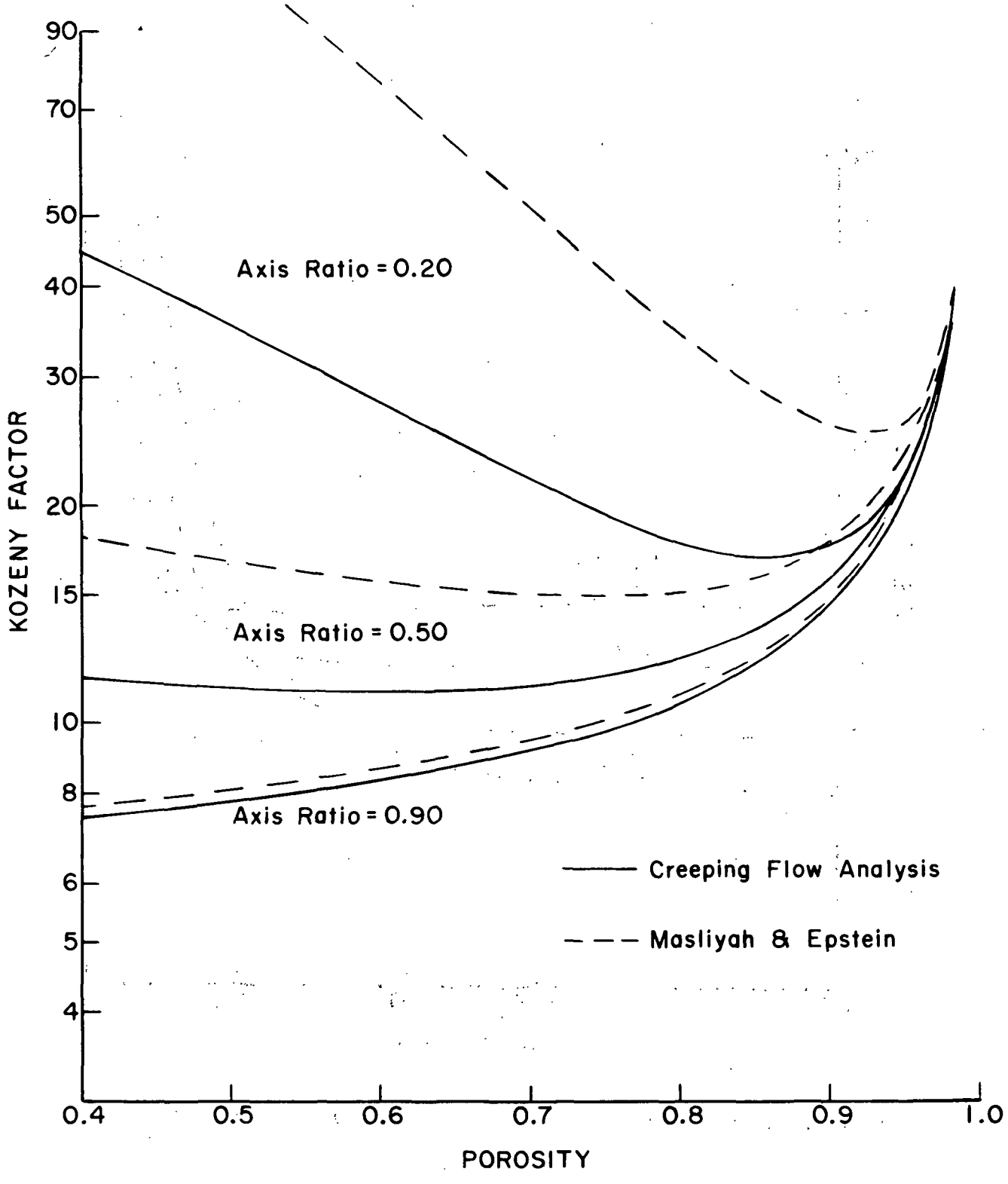

Fig. 7. Comparison of Two Zero Vorticity Cell Model Analyses for Perpendicular Flow Along Minor Cross-Sectional Axis.

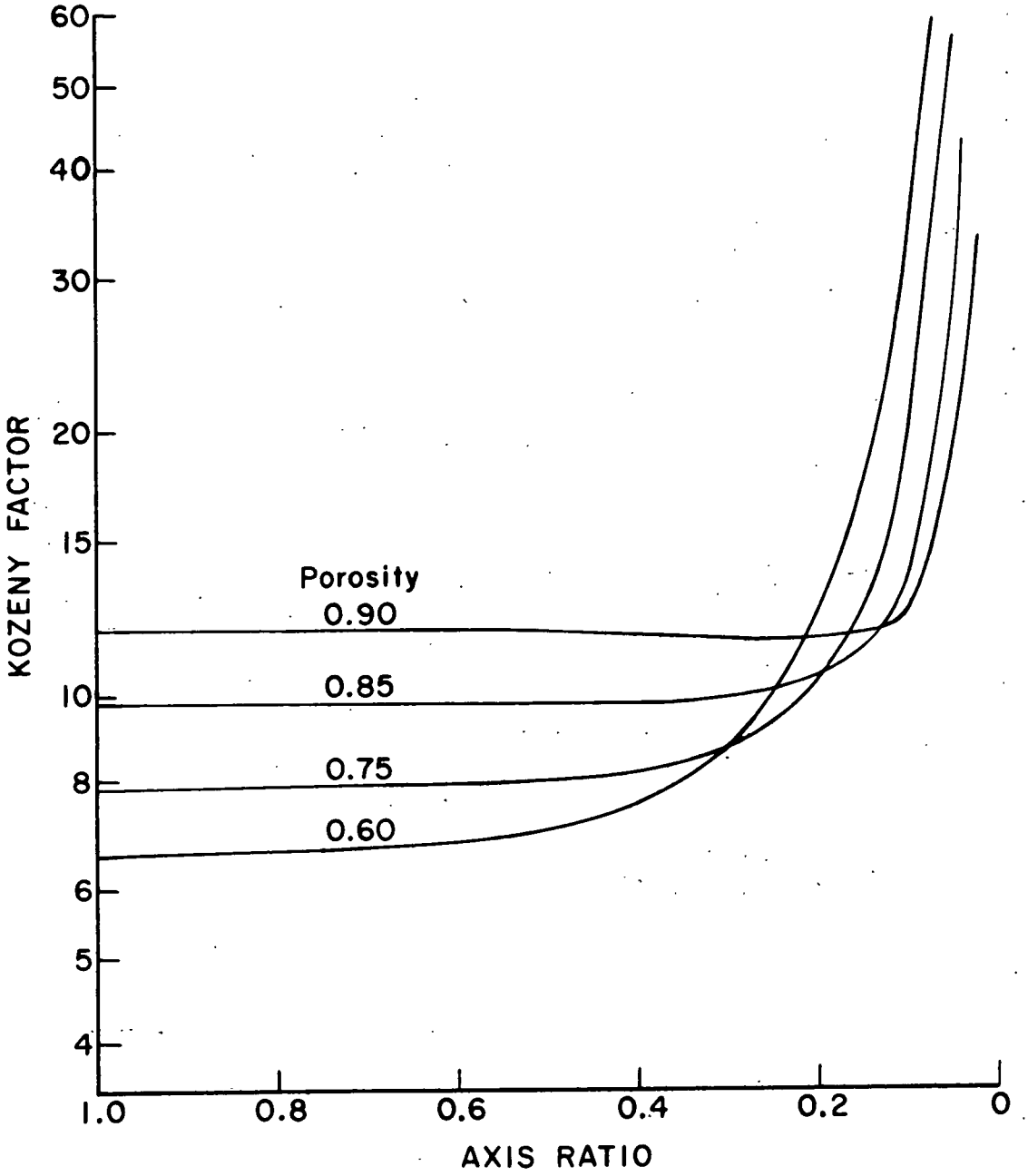

Fig. 8. Isotropic Mat Kozeny Factors as a Function of Axis Ratio.

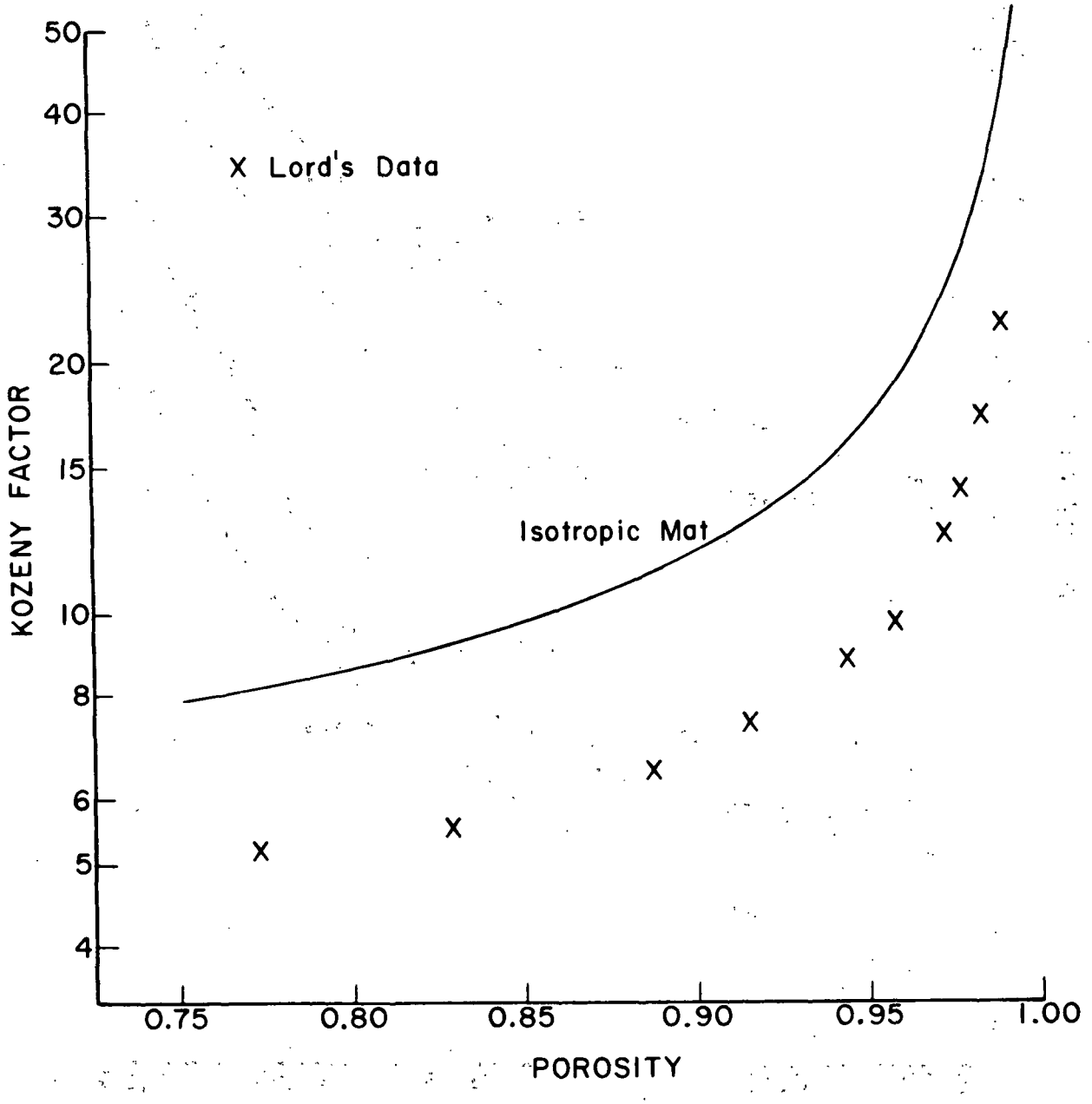

Fig. 9. Kozeny Factors for Isotropic Mat and for Randomized Beds of Silk Fibers.

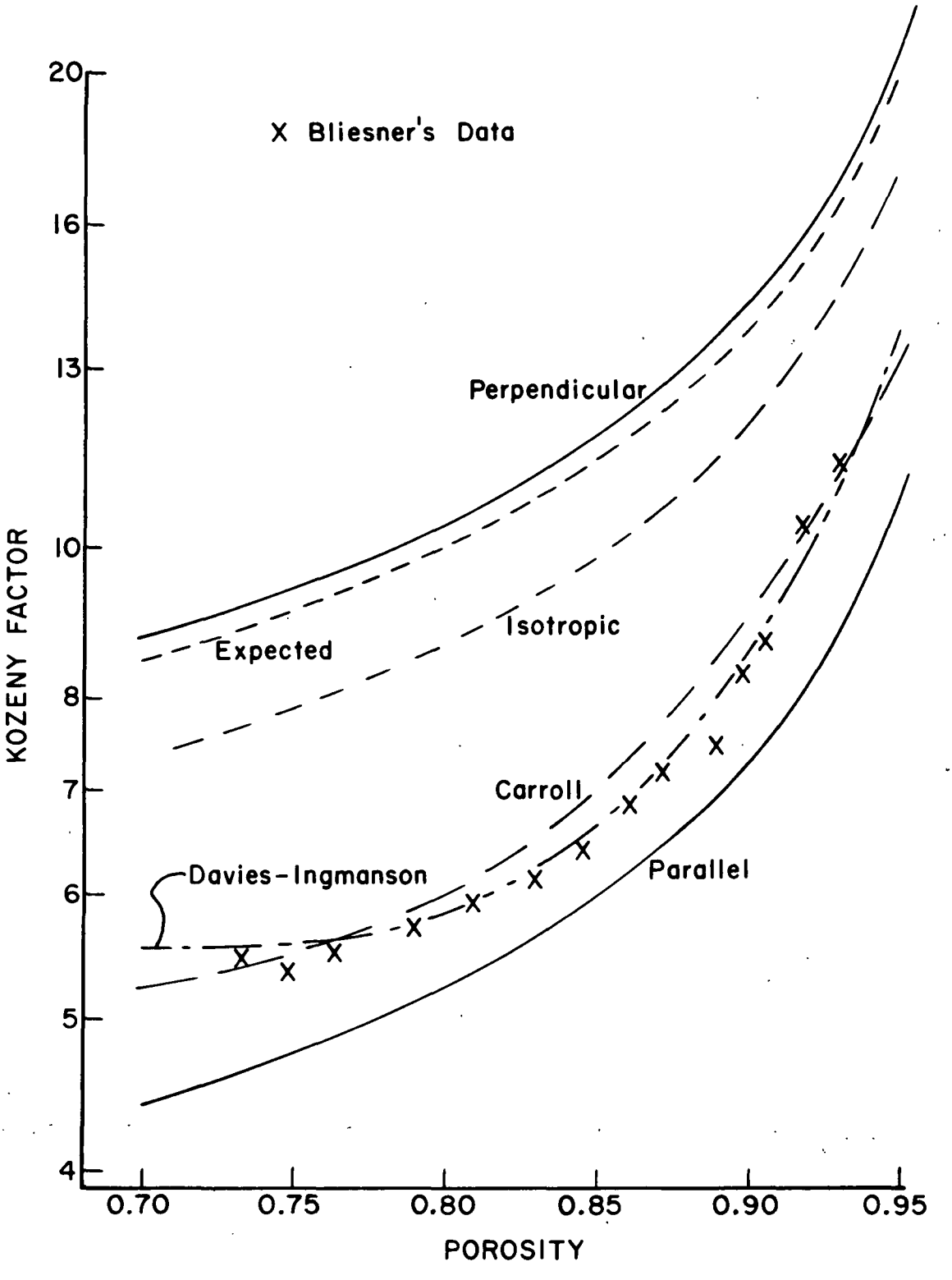

Fig. 10. Kozeny Factors for Circular Fibers: Analytical Values and Bliesner's Experimental Data.

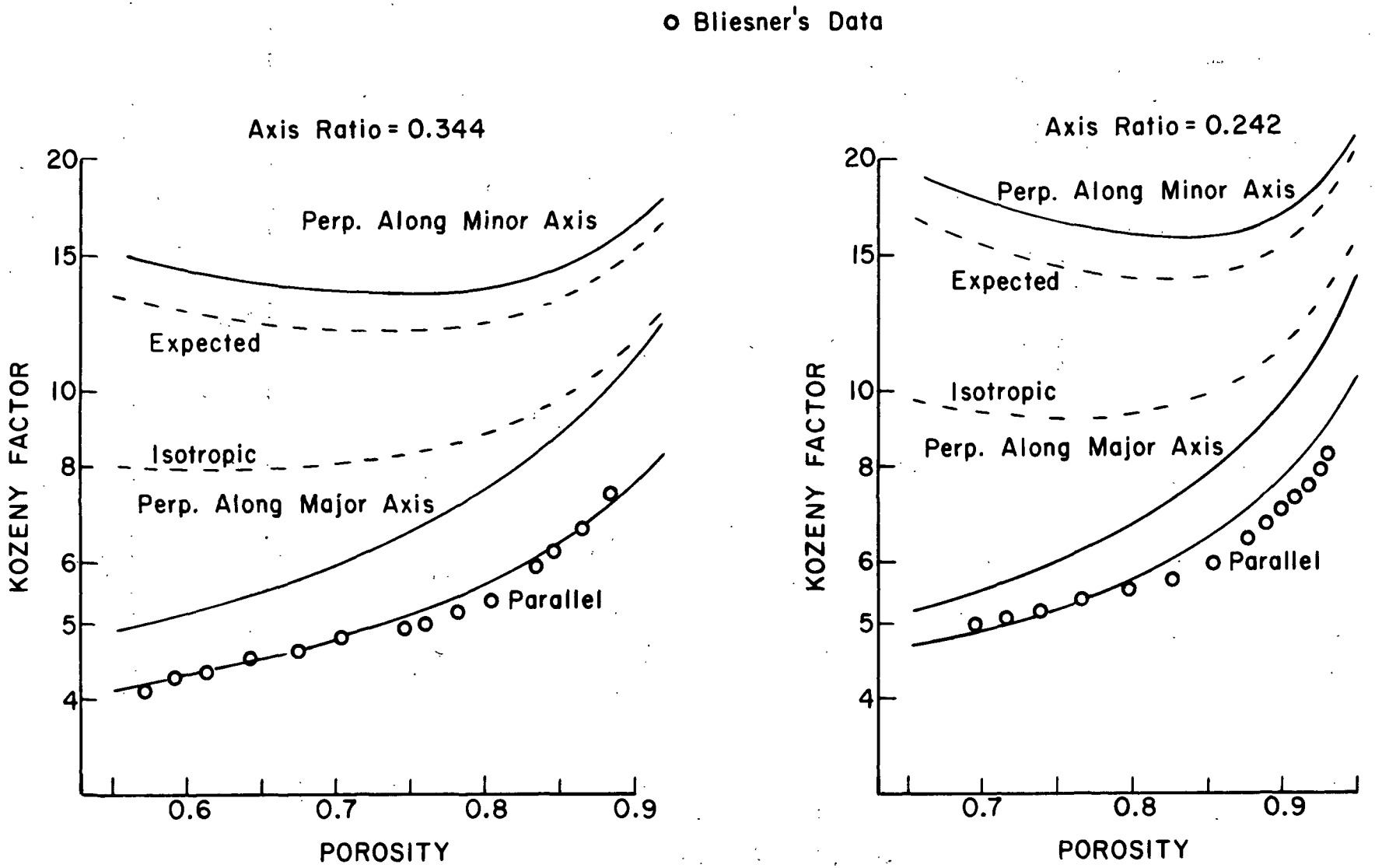

Fig. 11. Kozeny Factors for Noncircular Fibers: Analytical Values and Bliesner's Experimental Data.

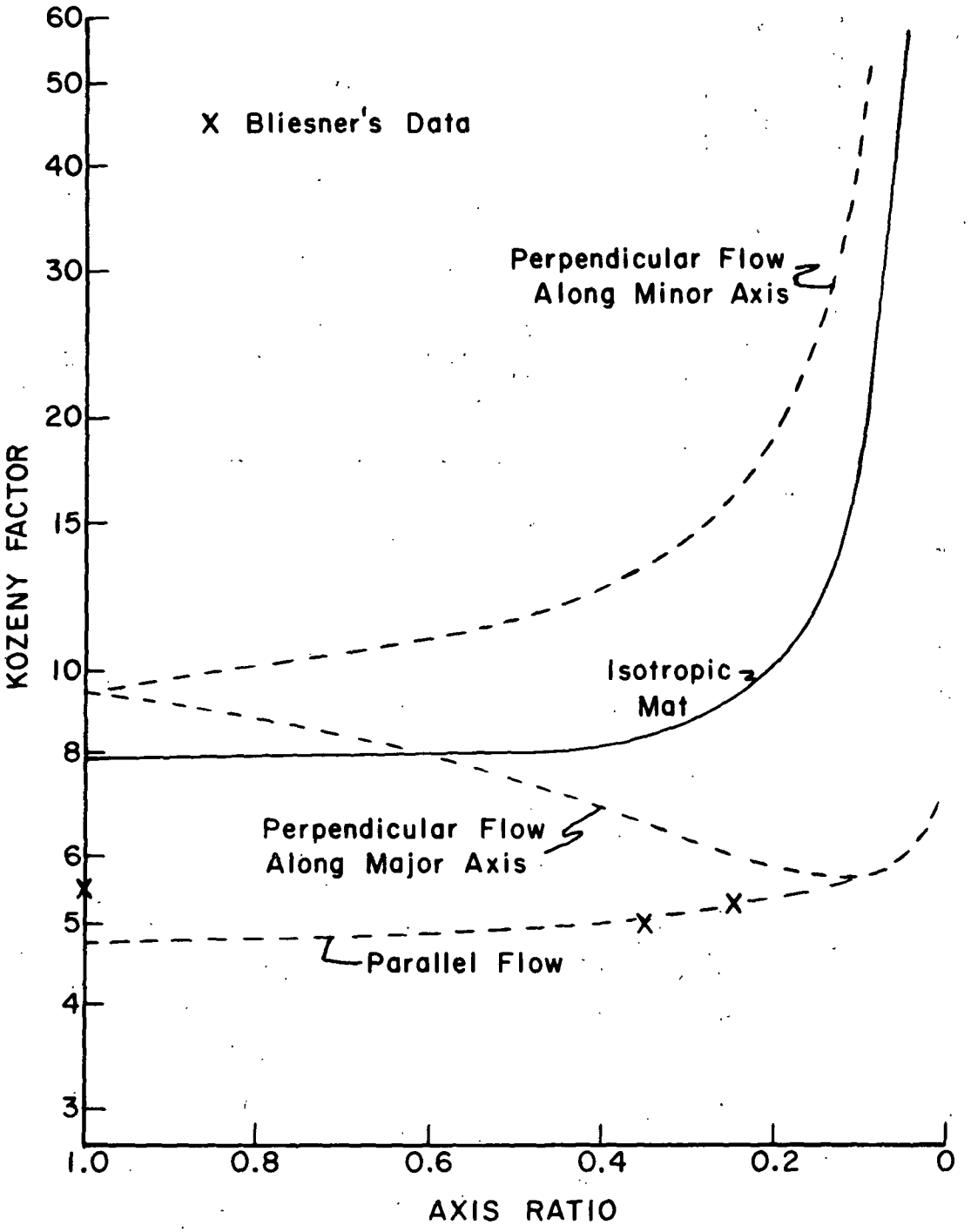

Fig. 12. Analytical and Experimental Kozeny Factors as a Function of Fiber Shape at Porosity 0.75.